Experimental plume characterization of a low-power Ablative Pulsed Plasma Thruster (APPT)

IEPC-2022-556

Presented at the 37th International Electric Propulsion Conference
Massachusetts Institute of Technology, Cambridge, MA, USA
June 19-23, 2022

Scherezade Barquero[1], Jaume Navarro-Cavallé, and Mario Merino
Equipo de Propulsión Espacial y Plasmas (EP2), Universidad Carlos III de Madrid, 28911 Leganés, Spain

An under-20 J ablative pulsed plasma thruster for CubeSat and small satellite applications is characterized experimentally. Voltage in the thruster main electrodes and in the spark plug circuit are measured to assess the repeatability of the discharge. A set of plasma probes placed downstream from the device are used to estimate the velocity of ion groups and the divergence rate of the exhaust as a function of the capacitor bank voltage. Finally, a novel diagnostic setup consisting in a grid of wires is proposed to resolve the time-varying cross sectional profile of the plasma ejecting from the thruster.

I. Introduction

Ablative Pulsed plasma thrusters (APPT) are electromagnetic space propulsion systems [1]. While different geometrical configurations of APPT exist, in essence, the APPT consists of a pair of parallel electrodes (cathode-anode) which shapes a channel-like configuration. On one end, the solid propellant, typically PTFE, is embedded in between the electrodes. The surface layer of this propellant is ablated and ionized by applying a large cathode-anode voltage, V_0. At the order of magnitude of the nominal V_0, this process needs to be triggered by an igniter, which will be further discussed in next sections. Once the main plasma is generated, a net anode-cathode current is established. This current that interacts with the self-induced magnetic field results in the Lorentz force, which accelerates the plasma down the channel, until it is ejected. Fig. 1 shows an APPT discharge sequence to illustrate the description above. In contrast to other plasma thrusters, this technology is suitable for low power operation (constraining the maximum pulsing frequency allowed by the power circuit) and miniaturization, which constitutes an opportunity for nanosatellites to have on-board propulsion. Nevertheless, some drawbacks are also involved, as the demands imposed on the electromagnetic compatibility of nearby devices, or the lifetime reliability of the ignition due to erosion and contamination issues.

Since the 60s, multiple research groups have been working worldwide on systematic studies of APPTs at different energy levels. However, the efforts to describe the discharge physical mechanisms in detail have been so far limited [2, 3]. Among other aspects, the nano- and microsecond characteristic time scales involved, together with the peculiarity of dealing with a multi-species pulsed plasma, stand as major difficulties. Hence, many challenges still prevail concerning the understanding of the APPT discharge, the underlying physics and the influence of geometrical and operational design parameters.

Relevant time-of-flight studies were carried out on the LES-6 and LES-8/9 APPTs by R.J. Vondra, K.I. Thomassen and A. Solbes [4], and N. Gatsonis, R. Eckman and others [5] respectively. Two ion populations with maximum velocities around 60 km/s and 30 km/s were identified for different operation regimes, including the low energy one, below 5 J (note that available energy is defined as ½ CV_0^2). Most recent experimental results corroborating these orders of magnitude have been published, e.g., by W.Y.L. Ling et al. [6] or by G. Pellegrini and others [7]. Some works were also extended in association to spectroscopy. Hence, additional studies at the LES-6 plume identified multiply ionized species of carbon and fluorine atoms, which were able to be related with velocities of $C^+ \sim 5-20$ km/s, $C^{2+} \sim 20-30$ km/s, $C^{3+} \sim 30-40$ km/s, $F^+ \sim 5-15$ km/s, $F^{2+} \sim 15-20$ km/s, and $F^{3+} \sim 20-30$ km/s [8].

The characterization of the time-varying exhaust shape of the APPT is relevant not only due to the direct effect of plume divergence on the efficiency of the device, but also in relation to its integration inside satellite platforms, where

[1] mbalsera@ing.uc3m.es

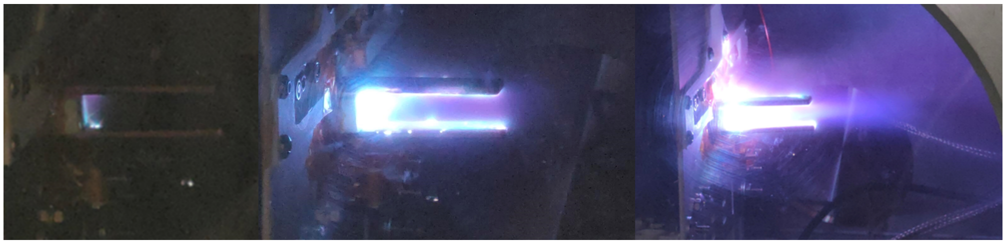

(a) LWCIDx Nominal channel size (see Section II).

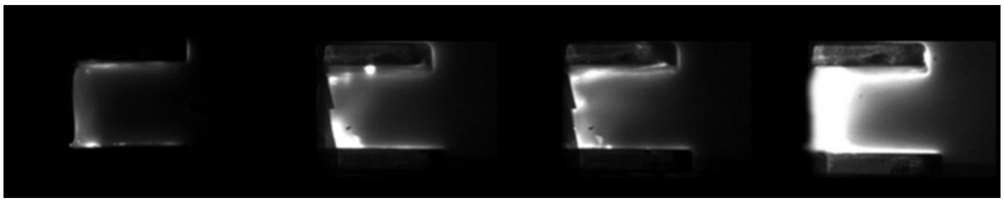

(b) Shorter electrodes.

Fig. 1 APPT discharge sequences by means of photography.

the interaction of the energetic plasma with neighboring surfaces poses a major contamination and erosion issue. To date, no systematic study of the cross-sectional shape of the plasma exhaust of the APPT has been performed, to the best knowledge of the authors.

In this work, a novel APPT breadboard model named LWCIDx, breech-fed and parallel-rail, is being developed in the frame of the regional MARTINLARA project. An experimental evaluation of the operation of LWCIDx has been carried out, aimed to (1) validate ignition, (2) ensure repeatability of the discharge, and (3) measure the velocity of the different ion groups being expelled from the thruster. These objectives are addressed by means of fast sampled (100 MHz) electrical measurements and probes located along the plume expansion axis. Additionally, (4) a fourth goal aims to assess the cross-sectional shape of the transient exhaust as a function of time. A parametric study of the main electrodes discharge voltage, V_0, from 500 to 2500 V (equivalent to 0.75 – 18.75 J), is performed for the three objectives mentioned above.

The rest of the document is structured as follows: Section II presents the LWCIDx APPT prototype and the experimental setup; Section III focuses on the analysis of the plasma discharge and the characterization different ion groups velocity. Finally, Section IV presents the development of the probe grid system for the measurement of the transient plume shape and illustrates some preliminary results. Conclusions and an outlook of future work can be found in section V.

II. Experimental setup and methodology

A. LWCIDx APPT prototype

The operation of a low-power class breech-fed and parallel-rail-electrode APPT breadboard model, named LWCIDx APPT –LoW-power Consumption In-space Device, x version– and shown in Fig. 2, has been experimentally studied in this work. Its design is the result of several previous iterations [9, 10].

The device features a nominal discharge chamber of 4.5 cm length (l), 1 cm height (h), 1 cm width (w), and equally-sized electrodes made of copper with the cathode grounded. Besides, the mentioned geometry can be easily modified, since the prototype has been designed under the requirement of being reconfigurable and modular. A block of PTFE is used as propellant. In the rear part of the thruster a main capacitor bank of 6 μF capacitance is connected to the (A/C) electrodes. This capacitor bank, which is charged externally by a specific DC-DC converter, provides the electrical power to the main discharge. The nominal discharge voltage is 1 kV, resulting in a discharge energy of 3 J. The firing frequency is set to 0.1 Hz to enable all the acquired data to be saved between shots.

In this work it is performed a parametric study on the initial main capacitor bank voltage V_0 from 500 V to 2500 V, with steps of 250 V. As the thruster capacitance is kept constant at 6 μF, this corresponds to the energy range from 0.75 J to 18.75 J.

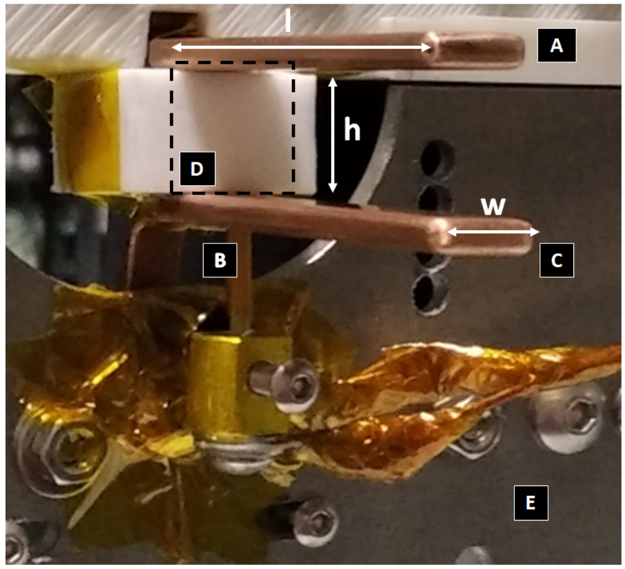

Fig. 2 Discharge channel of LWCIDx. "A" refers to the anode, "C", the cathode, "D", the effective propellant surface (PTFE), and "E", the thruster platform which holds the discharge chamber. Concerning dimensions, l, h and w mean channel length, height and width, correspondingly.

Once the main capacitor bank is charged up, ignition is triggered by a 1.5 kV Metal-Insulator-Metal (MIM) spark plug (tungsten electrode and PTFE as dielectric filler) developed in-house. This is placed close to the main propellant surface through a hole in the cathode electrode (i.e., the second Metal). The tungsten rod is negatively biased with respect to the cathode electrode. This ignition system is shown in Fig. 2, was tested in the past year to ensure reliability for more than 5000 shots[9, 10].

The thruster is operated inside HEDRON, a 50 cm-edge cubic vacuum chamber at the EP2 laboratory. MHV feedthroughs are used to power the thruster and BNC ones for the diagnostic probes. The vacuum system of Hedron consists of a mechanical vacuum pump (Edwards nXDS Scroll pump, 10 m^3/h) and a turbomolecular pump (Edwards next400, 400 L/s (N_2)). The ultimate pressure 10^{-6} mbar, perturbed at each firing to less than $2 \cdot 10^{-5}$ mbar. Pressure drops to the ultimate level in a few seconds after each firing.

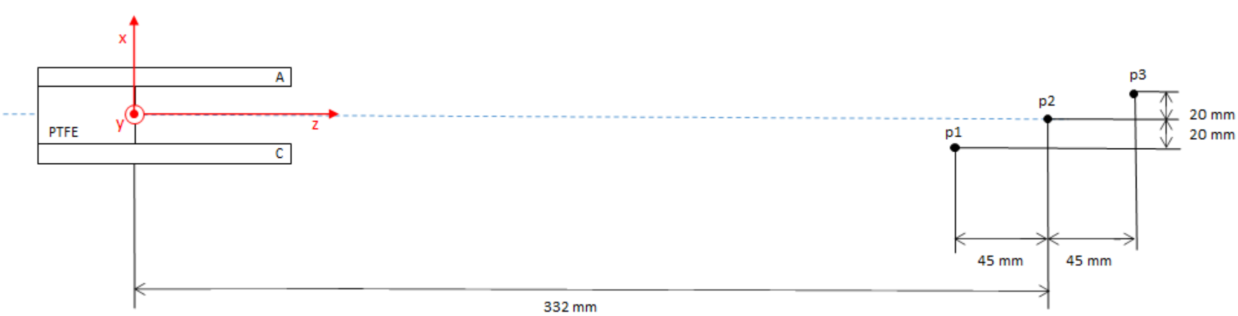

Fig. 3 Experimental setup for time-of-flight Langmuir probes p1, p2 and p3 –not to scale. "A", anode, and "C", cathode.

B. Electric and time-of-flight diagnostics

An eight-analog-channels Yokogawa DLM5000 oscilloscope is used to measure. The oscilloscope sampling frequency is 100 MHz. Teledyne LeCroy High voltage passive probes were used for voltage monitoring of the triggering and main discharge batteries –the APPT circuit remains outside the vacuum chamber. Concerning the plasma probes, these are, essentially, Langmuir probes (LP), and are exposed to the plasma plume at different locations as it will be discussed next.

In this work, The time-of-flight technique will take as input the time-resolved current measured by three different LPs placed smartly along the plume expansion (see Fig. 3 for further details). LPs are biased negatively to work well inside the ion saturation regime (-50 V at least). These are made of tungsten, and are elongated cylindrical rods of 0.508 mm diameter and 190 mm long.

As a result, being the spacing between LP i and j, Δz_{ij}, and the measured time delay between the corresponding peaks, Δt_{ij}, then the estimated ion velocity is $v_{ij} \simeq \Delta z_{ij}/\Delta t_{ij}$.

III. Results

A. Discharge characterization

In this section we analyze the discharge sequence of the APPT. The voltage response at the main capacitor battery has been measured as a function of the channel initial voltage V_0. Multiple realizations at the nominal V_0 (1000 V) are shown in Fig. 8b. The voltage response is underdamped and exhibits an oscillation with frequency in the order of 100 kHz before decaying to zero. The RC constant of the discharge signal envelope is equal to $-2.5825 \cdot 10^{-6}$. Superimposed to the mentioned oscillation there is a high frequency component taking place during the first instants of the ignition. This higher frequency oscillations are associated to the electromagnetic noise of both, the spark plug and that generated during the breakdown of the discharge. At values of V_0 around 1 kV, the voltage response exhibits good repeatability among pulses. As V_0 is decreased or especially as it is increased, the repeatability of the later oscillation periods is reduced. The variation of the voltage response with initial voltage V_0 is illustrated in Fig.4b. As it can be noted, the response is qualitatively the same as in the nominal case.

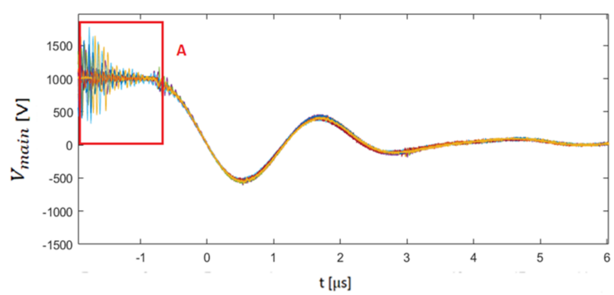

(a) Main discharge voltage waveform for multiple thruster firings. Region "A" highlights the pre-breakdown stage (between the triggering discharge (spark plug discharge) and the time at which impedance collapse of the main battery occurs).

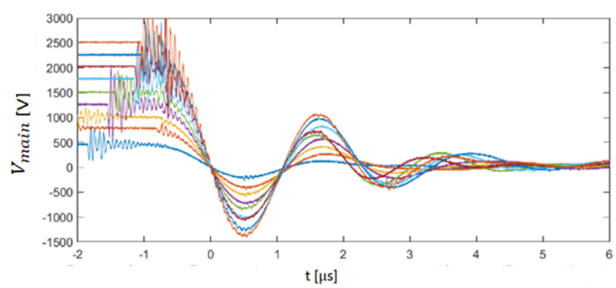

(b) Main discharge voltage waveform as a function of the initial channel voltage (V_0).

Fig. 4 APPT discharge electrical characterization.

To further investigate the initial instants of the discharge, Fig. 5a displays the voltage at the spark plug capacitor battery as a function of time. The response is likewise underdamped, albeit with a faster oscillation frequency in the order of 10 MHz. Remarkably, the voltage at which the breakdown in the spark plug initiates varies substantially among firings; this translates into a non-negligible statistical dispersion.

With the exception of the mentioned difference, the voltage response of the spark plug exhibits overall good repeatability in the first periods of the oscillation.

There is a small delay between the breakdown at the spark plug and at the main electrodes This delay is shown in Fig. 5b. As it can be observed, the delay decreases with V_0, and also involves a shot-to-shot variability that decreases with V_0.

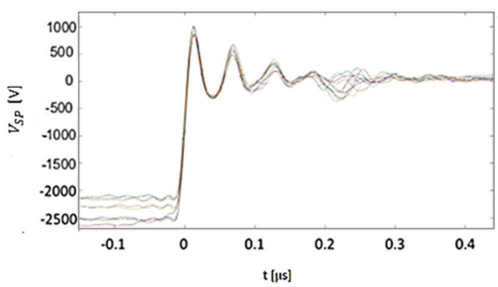

(a) Spark-plug voltage waveforme for multiple firings. Note that the voltage at breakdown $V_{sp,0}$ might change, being one of those parameters that lacks of repeatability.

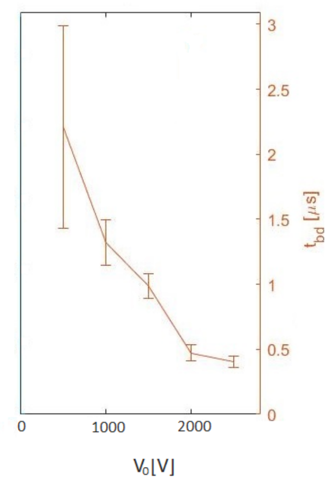

(b) Influence of the V_0 on the pre-breakdown lag time t_{bd}.

Fig. 5 Characterization of the APPT discharge triggering.

Lastly, coming back to Fig. 1 located in Section IV, it shows the discharge sequence in the APPT channel by means of photography. The initial discharge evolves from a plasma seed towards the anode, leading to the ignition of the main channel, which then forms a plasma that propagates downstream. The cross-channel plasma profile is non-uniform, concentrating at the electrode edges. Erosion/deposition patterns after multiple firings agree with this qualitative finding [10]. Canting of the plasma sheet and some hot spots on the electrodes are also visible.

B. Ion velocity: time-of-flight results

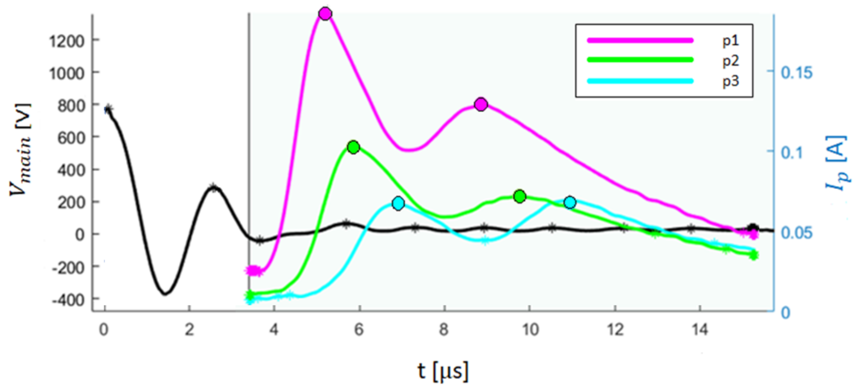

Fig. 6 Ion saturation current waveforms measured by the ToF probe set.

Fig. 6 shows an example of the current measured at the LPs for $V_0 = 750$ V. Probes data is shown for $t > 3.5$ μs, after an initially noisy interval that is discarded for the analysis. In this time interval, two or more current peaks can be easily distinguished in the three probes, separated to each other by about 5 μs. In spite of the good repeatability of the voltage signal discussed in section III.A, the ion saturation current measured at the probes showed a moderate variability. Datasets with unclear peaks, or with outlying probe values, have been discarded in the following analysis.

The observed peaks are hypothesized to correspond to two different ion populations, either because they are generated at different times or because they have a different charge/mass ratio and are accelerated differently in the expansion. The first peak is generally larger and has a higher associated velocity than the second one.

The resolution of the first peak improves at lower discharge voltage, while that of the second peak improves at larger voltages. For this reason, figure 7 displays the computed velocity of each peak in a different voltage range. These velocities are $51 \pm < 0.5$ km/s for the first ion population and $33 \pm < 4.5$ km/s for the second one for all discharge voltages, V_0. Therefore, it was not possible to identify any trends with V_0 under acceptable error in this experimental study. These values are in agreement with the reported ion speeds by other authors, as A. Solbes et al. [4] or N. Gatsonis and others [5].

The fact that increasing V_0 does not lead to a clear increase in the computed ion velocity suggests that the energy increment associated with larger V_0 may go either to a larger production of plasma or lost as heat or other losses in the device. Fig. 8 displays the peak current measured at probe 1 as a function of V_0 for each of the two ion groups. Since the first ion current peak increases with V_0, at least part of the extra energy is indeed increasing the production of the plasma associated with this peak. The value of the second peak, on the other hand, shows little dependency on V_0.

Finally, a first estimate about the LWCIDx plume area expansion rate can be obtained as follows. For a quasi-one dimensional expansion, the product of the ion current density (proportional to the current measured at the probes) and the plume area is constant, $j_i A = \text{const}$. Hence, the area variation rate can be approximated as $\mathrm{d}\ln A/\mathrm{d}z = -\mathrm{d}\ln j_i/\mathrm{d}z$. With this, at the example case of $V_0 = 750$, $\mathrm{d}\ln A/\mathrm{d}z \approx 1.3$.

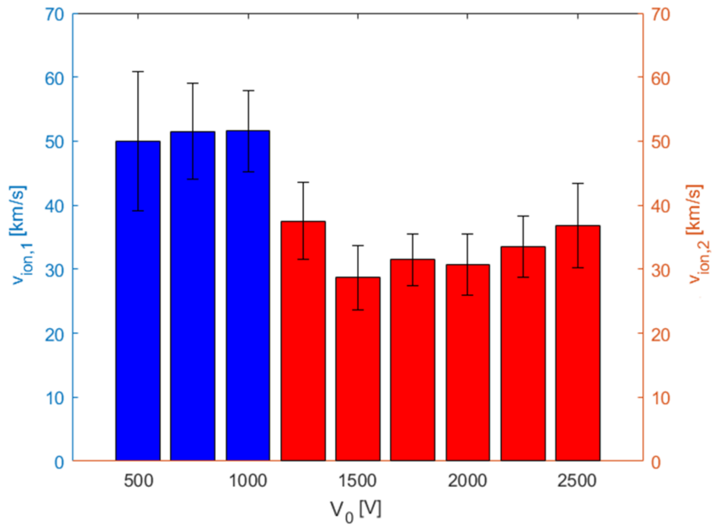

Fig. 7 Time of flight results: velocity of ion populations 1 and 2 at different V_0. The figure shows constant speeds for each one of the ion groups. Ion population 1 was characterized with data at $V_0 < 1250$ V, and the ion population 2 with $V_0 > 1250$ V, where the corresponding time windows for each population systematically provide clearer data.

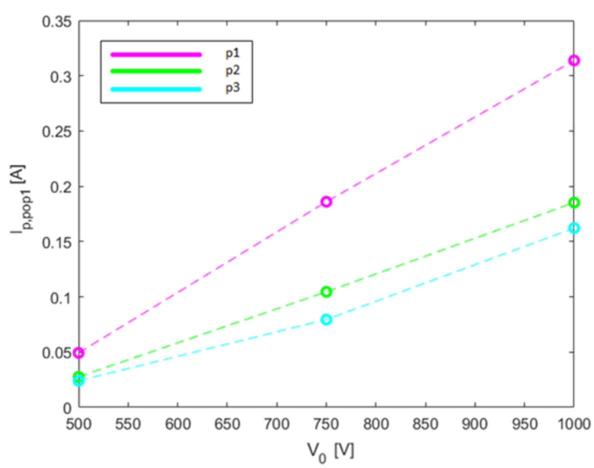

(a) Ion saturation current peaks for each one of the ToF probes for the ion population 1, as a function of V_0.

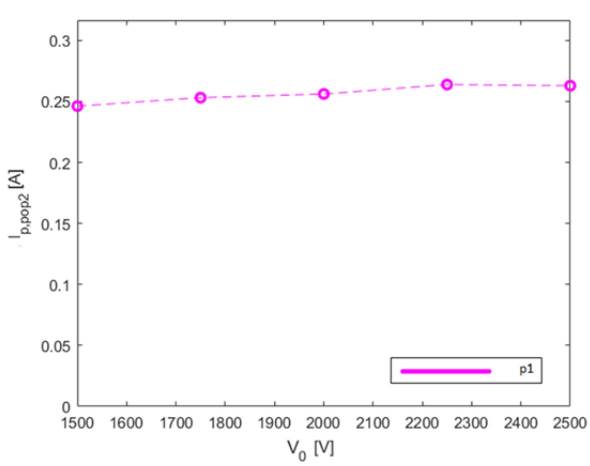

(b) Ion saturation current peaks for ToF probe 1 for the ion population 2, as a function of V_0.

Fig. 8 Peak ion saturation current variation with V_0 for ion populations 1 (left) and 2 (right). The variation of I_p for ion population 2 at probes 2 and 3 falls into the error margin of the measurements, and hence, has been ignored.

IV. Time-resolved plume profile diagnostic

As the last objective of this work, a dedicated probe grid diagnostic has been developed to measure the time-resolved cross sectional profile of the transient thruster exhaust. The new diagnostic system consists of a 20×20 cm frame that holds a series of independent horizontal and vertical probes in the xy plane, as shown in figure 9. The probes are naked tungsten wires of 19 cm length and 0.502 mm diameter; a separation of 1 cm is left between the vertical probe plane and the horizontal probe plane. The frame itself is grounded, and probes are insulated respect to it using fitted PTFE tubes. These probes are negatively biased to be within the ion saturation current regime, and the current to each probe can be measured simultaneously on a resistor bank. Coaxial wires are used in order to minimize noise. In the current setup, up to 7 probes can be sampled simultaneously, limited by the number of oscilloscope channels.

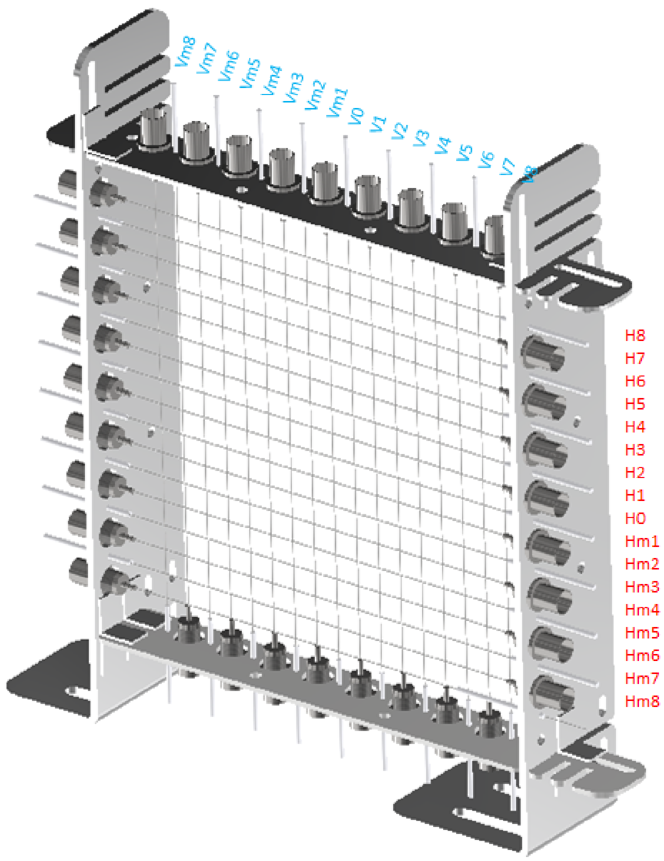

Fig. 9 Grid setup for time-resolved plume profile diagnostic.

The collected data consists of time-dependent integral current measurements along lines in the xy plane, at a fixed z location with respect to the channel. To resolve the cross-sectional ion current density profile at each time t, an inverse problem must be solved, analogous to other computed tomography (CT) problems.

The algorithm developed for this objective is briefly described next. Consider n_H wire probes parallel to the y direction and n_V wire probes parallel to the x direction. Each probe measures the integral ion current measured in an area defined by the probe length, its width, and the sheath thickness surrounding it:

$$H_i = \int j_i(x, y, t)\mathrm{d}x\mathrm{d}y, \qquad i = 1, ..., n_H \tag{1}$$

$$V_i = \int j_i(x, y, t)\mathrm{d}x\mathrm{d}y, \qquad i = 1, ..., n_V \tag{2}$$

For simplicity, in this preliminary stage of work, an axisymmetric gaussian profile is prescribed for the current density,

$$j_i(x, y, t) = C \exp(-r^2/2\sigma), \tag{3}$$

where r is the radius from the centerline of the thruster, and $C(t)$ and $a(t)$ are two functions of time to be determined. Naturally, more advanced fittings (e.g. different profiles in x and y, profiles displaced from the centerline) are possible. Up to $n_H + n_V$ degrees of freedom can be determined from the available data; if there are more data than 2 (for C and a), minimum squares can be used to optimize the representation of the plume.

For illustration purposes, figure 10 offers a visualization of the ion saturation current collected by the probe grid in an example firing, with the following wires present, H0, H6 and H13 (see Fig. 9), at $z = 332$ mm.

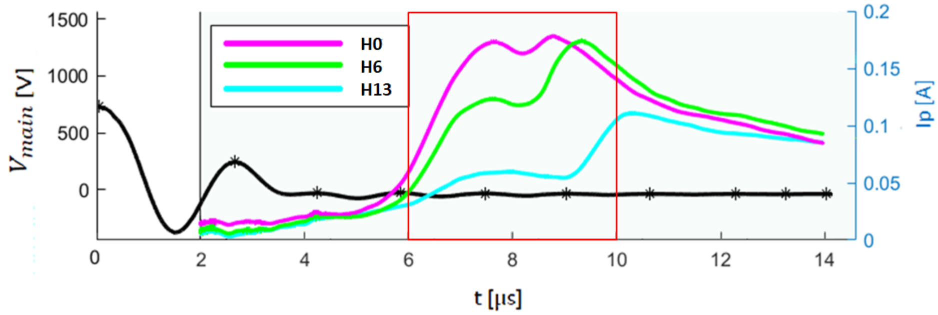

Fig. 10 Example of time-resolved plume cross section data. The probe currents are shown. The red square is positioned over the time interval at which j_i is analyzed in Fig. 11.

The coefficients $C(t)$ and $\sigma(t)$ of the ion current density fit in equation (3) are shown in Fig. 11 from 6 to 10 μs. Coefficient $C(t)$, which reflects the value of the peak of j_i, increases initially, then stabilizes up to $t = 9$ μs. Simultaneously, $\sigma(t)$ decreases and then stabilizes. Up to this instant in time, these results suggest that the plasma jet starts with a low peak value of the ion current density and a relatively large cross sectional area; then, it increases in magnitude and focuses. Finally, after $t = 9$ μs, the current measured at probe H6 becomes larger than at the central probe H0, signaling that the ion current density profile stops being single-peaked and evolves into a more complex structure. At this point, the Gaussian approximation used in this analysis fails, and a more advanced fitting procedure is needed.

Future work must (1) explore other fits to the ion current density profile that are not single peaked, nor axisymmetric, and (2) measure with more wires simultaneously both in the x and y directions.

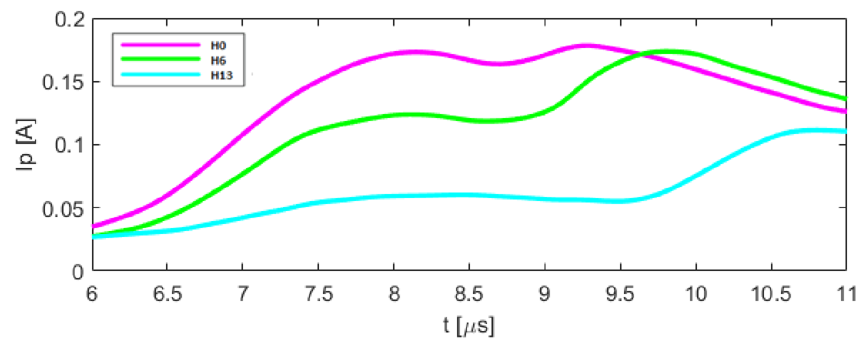

(a) Recorded data within the region interest.

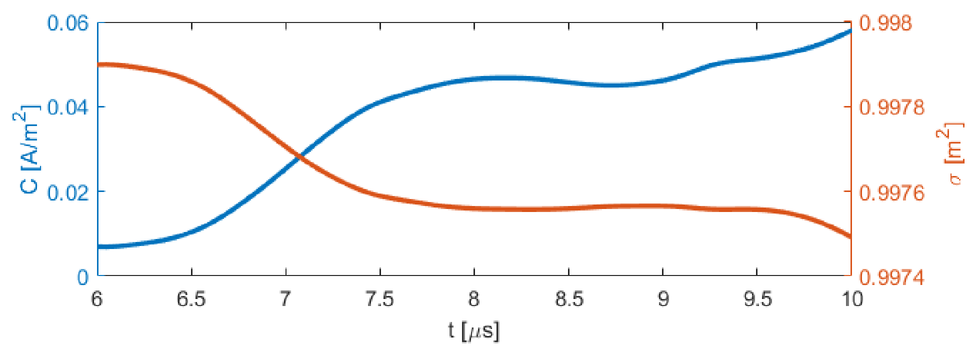

(b) Axisymmetric gaussian fitting to build $j(x, y, t)$.

Fig. 11 time-resolve the plume cross-sectional ion current density.

V. Conclusion

The discharge of a small ablative pulsed plasma thruster prototype has been characterized. The ion velocity in the plume has been studied with the time of flight between three probes located downstream. Finally, a novel plume shape diagnostic has been developed and described.

The voltage response at the main and spark plug capacitor banks have been analyzed, showing that the main aspects of the underdamped response are highly repeatable, at least in the first oscillation periods. The sensitivity of the breakdown voltage and the delay in the initiation of the main discharge with the main capacitor initial voltage V_0 has been documented.

Two ion populations have been identified, travelling at constant speed across the plume at about 50 km/s and 30 km/s respectively. No clear dependence with V_0 has been found, but results suggest that increasing the discharge energy by increasing V_0 translates into a larger plume current of the first ion group.

The on-going test campaign plume aims to measure the current density cross-sectional profile using the new probe grid diagnostic. Preliminary results have provided the time-resolved axisymmetryc j distribution along the time interval which involves the peak perturbation of the probes, and exposed a rich and complex behavior of the plume profile, which evolves from single-peaked to double-peaked as time advances.

Planned next steps concerning the determination of the ion velocity will perform a parametric analysis with V_0 and the capacitance of the main bank, as well as channel geometry variations. On the other hand, regarding the grid diagnostic system, future work must explore other current density fits.

Acknowledgments

This work was been supported by the MARTINLARA project, funded by the Comunidad de Madrid, under Grant reference P2018/NMT-4333 MARTINLARA-CM.

References

[1] Jahn, R., *Physics of Electric Propulsion*, Dover, 2006.

[2] Ling, W. Y. L., Schönherr, T., and Koizumi, H., "Characteristics of a non-volatile liquid propellant in liquid-fed ablative pulsed plasma thrusters," *Journal of Applied Physics*, Vol. 121, No. 7, 2017, p. 073301.

[3] Zhao, Y., and Wu, J., "A review on plasma diagnosis technology of pulsed plasma thruster," *Journal of Physics: Conference Series*, Vol. 1952, IOP Publishing, 2021, p. 032087.

[4] SOLBES, A., Thomassen, K., and VONDRA, R. J., "Analysis of solid teflon pulsed plasma thruster," *Journal of Spacecraft and Rockets*, Vol. 7, No. 12, 1970, pp. 1402–1406.

[5] Gatsonis, N. A., Eckman, R., Yin, X., Pencil, E. J., and Myers, R. M., "Experimental investigations and numerical modeling of pulsed plasma thruster plumes," *Journal of Spacecraft and Rockets*, Vol. 38, No. 3, 2001, pp. 454–464.

[6] Ling, W., Zhang, Z., and Tang, H., "Progress in Fundamental Pulsed Plasma Thruster Research," *35th International Electric Propulsion Conference, Electric Rocket Propulsion Soc., IEPC Paper*, Vol. 140, 2017.

[7] Pellegrini, G., Mancini, E., Paganucci, F., and Andrenucci, M., "Development and Characterization of a Pulsed Plasma Thruster," *Space Propulsion 2018*, 2018.

[8] Thomassen, K. I., and Vondra, R. J., "Exhaust velocity studies of a solid Teflon pulsed plasma thruster," *Journal of Spacecraft and Rockets*, Vol. 9, No. 1, 1972, pp. 61–64.

[9] Barquero, S., Merino, M., and Navarro-Cavallé, J., "Design of an experimental ablative pulsed plasma thruster for micropropulsion," *Space Propulsion Conference 2021*, Association Aéronautique et Astronautique de France, March 17-19, 2021.

[10] Barquero, S., Merino, M., and Navarro-Cavallé, J., "Preliminary test campaign of an ablative pulsed plasma thruster for micropropulsion," *5^{th} International Workshop on Micropropulsion and CubeSats*, Toulouse (online), 2021.